

# Superconducting Diode Effect in Quantum Spin Hall Insulator-based Josephson Junctions

Benedikt Scharf

*Institute for Theoretical Physics and Astrophysics and Würzburg-Dresden Cluster of Excellence ct.qmats,  
University of Würzburg, Am Hubland, 97074 Würzburg, Germany*

Denis Kochan\*

*Institute of Physics, Slovak Academy of Sciences, 84511 Bratislava, Slovakia and  
Center for Quantum Frontiers of Research and Technology (QFort),  
National Cheng Kung University, Tainan 70101, Taiwan*

Alex Matos-Abiague

*Department of Physics & Astronomy, Wayne State University, Detroit, MI 48201, USA  
(Dated: June 14, 2024)*

The superconducting diode effect (SDE) is a magneto-electric phenomenon where an external magnetic field imparts a non-zero center-of-mass momentum to Cooper pairs, either facilitating or hindering the flow of supercurrent depending on its direction. We propose that quantum spin Hall insulator (QSHI)-based Josephson junctions can serve as versatile platforms for non-dissipative electronics exhibiting the SDE when triggered by a phase bias and an out-of-plane magnetic field. By computing the contributions from Andreev bound states and the continuum of quasi-particle states, we provide both numerical and analytical results scrutinizing various aspects of the SDE, including its quality  $Q$ -factor. The maximum value of the  $Q$ -factor is found to be universal at low (zero) temperatures, which ties its origin to underlying topological properties that are independent of the junction's specific details. As the magnetic field increases, the SDE diminishes due to the closing of the induced superconducting gap caused by orbital effects. To observe the SDE, the QSHI-based Josephson junction must be designed so that its edges are transport-wise non-equivalent. Additionally, we explore the SDE in a more exotic yet realistic scenario, where the fermionic ground-state parity of the Josephson junction remains conserved while driving a current. In this  $4\pi$ -periodic situation, we predict an enhancement of the SDE compared to its  $2\pi$ -periodic, parity-unconstrained counterpart.

## I. INTRODUCTION

Magneto-electric phenomena accompanying superconductors with broken time-reversal and space-inversion symmetries are attracting considerable attention.<sup>1</sup> There are numerous superconducting systems displaying the supercurrent diode effect (SDE) including (1) thin superconducting films,<sup>2-5</sup> (2) Josephson junctions (JJs) based on (i) semiconductors,<sup>6-11</sup> (ii) topological semimetals,<sup>12</sup> (iii) proximity-magnetized metals with strong spin-orbit coupling (SOC),<sup>13</sup> (iv) van der Waals heterostructures,<sup>14-16</sup> (v) twisted bilayer<sup>17</sup> and trilayer<sup>18</sup> graphenes, (3) Josephson weak links through a single magnetic atom<sup>19</sup> or even (4) altermagnets<sup>20,21</sup>. As many of them demonstrate potential for the supercurrent rectification, that is, maintaining a system superconducting for one current direction, while transiting it to resistive state for the opposite one, they digress in roles played by magnetic fields, Meissner screening, magnetization, the origin of spin-momentum locking, and generically in the spin-resolved spectral properties of the associated sub-gap states. All these nuances diversify the SDE and pin its origin with various proliferating adjectives like intrinsic, field-free,<sup>15</sup> universal,<sup>22</sup> single-atomic,<sup>19</sup> trivial, ubiquitous,<sup>5</sup> flux-tunable<sup>23</sup>, and altermagnetic<sup>20</sup>, among others.

There is a common agreement linking the SDE with an appearance of finite center-of-mass momentum of Cooper pairs, although, there is less consensus on what causes its non-zero value. The breakdown of time-reversal symmetry, triggered by a magnetic field (via Zeeman coupling) or magnetization (via exchange splitting), and a moving condensate while probing the supercurrent seem to be necessary ingredients in all scenarios.<sup>5-7,9-11,22,24-35</sup> However, there is still an ongoing discussion to which extent the SOC plays a role. Since experiments vary in terms of materials, geometry, measurements, and even the nature of superconductivity (whether intrinsic or proximity-induced), no single theory can comprehensively explain the SDE in all its various forms. The primary distinction between models of the SDE lies in their stance on SOC. Pro-SOC models<sup>6,7,9,10,24-31,36,37</sup> link supercurrent rectification to the emergence of a helical superconducting phase.<sup>24,25,38-41</sup> In contrast, con-SOC models<sup>5,22,32,34,35</sup> attribute the SDE either to a Doppler shift in the quasi-particle spectra for left and right movers or to diamagnetic effects resulting from stray fields and inhomogeneous screening, or alternatively to Yu-Shiba-Rusinov states<sup>19,42</sup>.

In this paper we scrutinize magneto-chiral properties of two-dimensional (2D) JJs based on Quantum Spin Hall Insulators (QSHI) and explore their abilities to fos-

ter the SDE when tuning an out-of-plane magnetic field, the phase biasing, and/or the edge-channels asymmetry. We compute individual contributions to the supercurrent carried by the spin-resolved Andreev bound states (ABS) and the continuum quasi-particle states, and analyze their roles in the emergence of the SDE. Using a minimal yet realistic model capturing the main junction characteristics and considering the relevant system parameters, we investigate the SDE and provide practical analytical formulas for the underlying quality  $Q$ -factor, focusing primarily on its dependencies on magnetic field and temperature. We show that in the presence of an out-of-plane magnetic field and at very low temperatures the maximum of the  $Q$ -factor acquires a universal value, which is independent of the junction parameters. Finally, we show that the SDE and its corresponding  $Q$ -factor can be further enhanced by considering  $4\pi$ -periodic junctions where the fermionic ground-state parity remains conserved while probing the supercurrent, which requires a measurement of the SDE on timescales shorter than the quasi-particle poisoning time.

The paper is organized as follows: In Sec. II we present the model Hamiltonian and discuss the associated Andreev and continuous spectra and their corresponding density of states. In Sec. III we study the underlying free energy and Josephson current and their dependencies on temperature and magnetic field, among other junction parameters. The effects of the magnetic field, edge-state Fermi velocities, and temperature on the properties of the SDE and  $Q$ -factor in QSHI-based 2D junctions are analyzed in Sec. IV. Section V is devoted to the discussion of the SDE when the fermionic ground-state parity is conserved. We examine possible ramifications toward experimental realizations of the SDE in QSHI-based JJs in Sec. VI. After the concluding remarks, the paper is supplemented with two brief technical Appendices.

We use standard notations throughout this paper, where  $e > 0$  stands for the elementary charge,  $\Phi_0 = h/e$  is the quantum of the magnetic flux, and  $k_B$  is the Boltzmann constant. Additionally,  $\Theta(x)$  and  $\text{sgn}(x)$  denote the Heaviside step function and sign function, respectively.

## II. MODEL, ANDREEV BOUND STATES AND CONTINUUM DENSITY OF STATES

We consider a short QSHI-based topological JJ employing the established  $\delta$ -function model developed in Ref. 43 (for the geometry and configuration see Fig. 1). We assume the Fermi level is tuned to the bulk gap of the QSHI. Hence the only propagating modes are the spin-polarized edge states. When the width  $\mathcal{W}_S$  of the junction is wide enough—as assumed in this paper—the QSHI edge states (referred to as the top and bottom edges/channels) do not overlap and their low-energy dynamics decouple. Correspondingly, the physics at each edge can be accurately described by the Bogoliubov-de

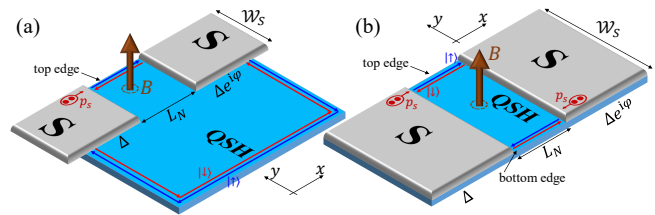


FIG. 1. Topological Josephson junctions formed by (a) one and (b) two QSHI edges. Here the QSHI is partially covered by two  $s$ -wave superconductors with different superconducting phases, the Cooper-pair tunneling induces superconducting proximity pairings in the corresponding regions of the QSHI, defining the superconducting (S) and normal (N) spacers. The N region is subtended by a perpendicular magnetic field  $\mathbf{B}$ . The coordinate system is chosen in such a way that the QSHI lies in the  $xy$  plane, with  $x$  being the transport direction defined by the gradient of the superconducting phase, correspondingly,  $\mathbf{B} = B\mathbf{e}_z$ . The edge with a positive (negative) ordinate  $y$  is called the top (bottom).

Genes (BdG) Hamiltonian,

$$\hat{H}_s^\sigma = (s\sigma v_F \hat{p}_x - \mu_S) \tau_z + s \frac{v_F p_S}{2} + V_0 h(x) \tau_z + \Delta [\tau_x \cos \Phi^\sigma(x) - \tau_y \sin \Phi^\sigma(x)]. \quad (1)$$

In the above equation,  $\hat{p}_x = -i\hbar\partial_x$  denotes the momentum operator,  $\mu_S$  represents the chemical potential in superconducting (S) regions,  $V_0$  is the potential difference between the normal (N) and S regions, and the (super/sub)scripts  $s = \uparrow/\downarrow \equiv \pm 1$  and  $\sigma = t/b \equiv \pm 1$  represent the spin projections along the  $z$ -axis and the top and bottom channels, respectively. Finally  $\tau_{x,y,z}$  are Pauli matrices operating on the particle-hole degrees of freedom. We consider junctions where the top and bottom edge states have the same Fermi velocity ( $v_F = v_F^{t/b}$ ), although junctions with  $v_F^t \neq v_F^b$  are also possible, as discussed in Sec. VI. We limit our study to short junctions, where the length of the N region  $L_N$  is shorter than the superconductor coherence length. Furthermore, we also assume  $L_N$  to be shorter than the Josephson penetration depth, such that Josephson vortices and Fraunhofer features do not affect the system under consideration. Therefore, the N region can be effectively modelled as a  $\delta$ -like spacer with a potential profile  $h(x) = L_N \delta(x)$ . The QSHI is proximitized by two  $s$ -wave superconductors which are assumed to have equal gap magnitudes, but different superconducting phases. Consequently, the induced superconducting pairing in the QSHI,  $\Delta e^{i\phi(x)}$ , retains a constant gap amplitude  $\Delta$ , but an  $x$ -dependent phase  $\phi(x)$ ,  $\phi(x < 0) = 0$  and  $\phi(x > 0) = \phi$ , resulting in a global phase difference  $\phi$ . An out-of-plane magnetic field  $\mathbf{B} = B\mathbf{e}_z$  with  $B \geq 0$  induces:<sup>44</sup> (i) an orbital Doppler shift described by the Cooper pair momentum  $p_S$  and (ii) the edge-selective superconducting-phase profiles  $\Phi^\sigma(x)$  with  $\Phi^\sigma(x < 0) = 0$  and  $\Phi^\sigma(x > 0) = \phi^\sigma$ ,

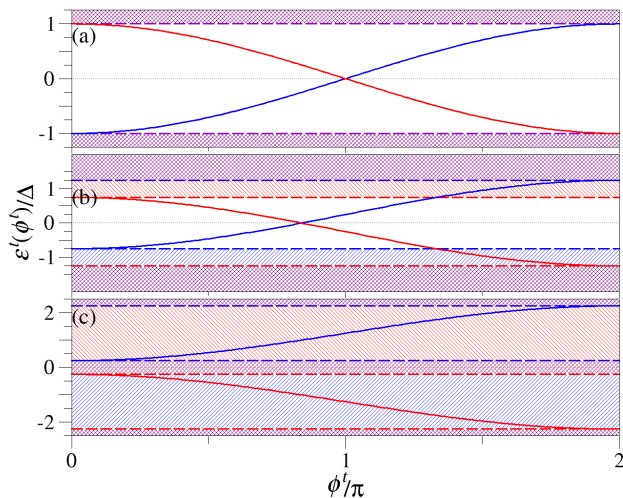


FIG. 2. ABS given by Eq. (3) for the top edge for different  $\gamma = v_F p_S / (2\Delta)$ : (a)  $\gamma = 0$ , (b)  $\gamma = 0.25$ , (c)  $\gamma = 1.25$ . Here the blue and red colors denote different spin quantum numbers  $s = \uparrow/\downarrow \pm 1$  associated with the sub-gap ABS (solid lines) and the supra-gap continuum states (shadings).

where

$$p_S = \pi \hbar \frac{B \mathcal{W}_S}{\Phi_0}, \quad \phi^\sigma = \phi + \sigma \frac{p_S L_N}{\hbar}. \quad (2)$$

The second term in  $\phi^\sigma$  can be interpreted as a kinematic phase acquired by a Cooper pair with a momentum  $\sigma p_S$  when traversing a distance of  $L_N$ .

Following Refs. 43 and 45, the ABS spectra associated with the model Hamiltonian, Eq. (1), are determined by means of the spectral scattering approach, which yields per each edge (indexed by  $\sigma$ ) two ABS branches (indexed by spin  $s$ ) with an obvious  $2\pi$  periodicity,

$$\epsilon_s^\sigma(\phi^\sigma) = s \left[ -\sigma \Delta \cos \frac{\phi^\sigma}{2} \operatorname{sgn} \left( \sin \frac{\phi^\sigma}{2} \right) + \frac{v_F p_S}{2} \right]. \quad (3)$$

When  $\phi^\sigma = \phi^{t/b}$  approaches an integer multiple of  $2\pi$ , a pair of the sub-gap ABS with opposite spin projections merges into the continuum of quasi-particle states, see Fig. 2, while a pair of ABS with the reversed spins splits off from the supra-gap states.

Complementary, the continuum of quasi-particles contributes to the supra-gap density of states (DOS) that can be separated into a phase-independent (shown explicitly later) and phase-dependent part. It is the latter, which is important for the computation of the Josephson current via differentiation of the free energy with respect to the superconducting phase difference. The phase-dependent part of the DOS, per spin and edge, can be compactly written as,

$$\rho_s^\sigma(\epsilon, \phi^\sigma) = \frac{s\sigma\Delta^2}{2\pi} \frac{\Theta(\epsilon_s^2 - \Delta^2) \operatorname{sgn}(\epsilon_s) \sin \phi^\sigma}{\sqrt{\epsilon_s^2 - \Delta^2} (\epsilon_s^2 - \Delta^2 \cos^2 \frac{\phi^\sigma}{2})} \quad (4)$$

with

$$\epsilon_s = \epsilon - s v_F p_S / 2. \quad (5)$$

Although  $\rho_s^\sigma(\epsilon, \phi^\sigma)$  can be negative, the total DOS, which also includes the phase-independent part, is always positive. As discussed in Ref. 43, a finite  $v_F p_S$  decreases the effective superconducting gap, which closes for  $|v_F p_S| \geq 2\Delta$ . However, for each spin species saddled by the opposite edges of the QSHI the superconducting gaps still remain open individually, and although energetically not overlapping, see Fig. 2(c), the bound and continuum states exist simultaneously on a spatial scale defined by the junction width  $\mathcal{W}_S$ .

### III. FREE ENERGY AND CURRENT

The ABS spectra, Eq. (3), and the supra-gap DOS due to continuum states, Eq. (4), allow us to determine the free energy from which the Josephson current and other thermodynamic quantities follow straightforwardly. As the edges of the QSHI-based JJ are dynamically decoupled, the total free energy turns into a sum of its top and bottom parts. Hence, in an equilibrium held at temperature  $T$  and magnetic field  $B \geq 0$  the free energy  $F^\sigma(\phi^\sigma, T)$  of the edge  $\sigma$  (more precisely its phase-dependent part) equals,

$$F^\sigma(\phi^\sigma, T) = -k_B T \left\{ \ln \left[ 2 \cosh \left( \frac{\epsilon_\uparrow^\sigma(\phi^\sigma)}{2k_B T} \right) \right] + \int_0^\infty d\epsilon \rho^\sigma(\epsilon, \phi^\sigma) \ln \left[ 2 \cosh \left( \frac{\epsilon}{2k_B T} \right) \right] \right\}. \quad (6)$$

Equation (6) consists of a discrete part due to ABS and of a continuum part, which integrates over the supra-gap DOS summed over both spin projections,

$$\rho^\sigma(\epsilon, \phi^\sigma) = \sum_{s=\uparrow/\downarrow} \rho_s^\sigma(\epsilon, \phi^\sigma). \quad (7)$$

As the superconducting phase difference  $\phi$  and the edge-saddled phase difference  $\phi^\sigma$  differ by just a shift, Eq. (2), the Josephson current carried by an edge  $\sigma$  is then calculated as,

$$I^\sigma(\phi^\sigma, T) = \frac{2e}{\hbar} \frac{\partial F^\sigma(\phi^\sigma, T)}{\partial \phi^\sigma} = \frac{2e}{\hbar} \frac{\partial F^\sigma(\phi^\sigma, T)}{\partial \phi}. \quad (8)$$

Inserting Eqs. (3) and (4) into the free energy  $F^\sigma(\phi^\sigma, T)$ , the Josephson current splits into ABS and continuum contributions,

$$I^\sigma(\phi^\sigma, T) = I_{\text{ABS}}^\sigma(\phi^\sigma, T) + I_{\text{cont}}^\sigma(\phi^\sigma, T). \quad (9)$$

Introducing the short-hand notations,

$$I_0 = \frac{e\Delta}{2\hbar}, \quad \gamma = \frac{v_F p_S}{2\Delta}, \quad \tilde{\Delta} = \frac{\Delta}{2k_B T}, \quad (10)$$

the current contributions read,

$$I_{\text{ABS}}^\sigma(\phi^\sigma, T) = I_0 \sin \frac{\phi^\sigma}{2} \times \tanh \left[ \tilde{\Delta} \left( \cos \frac{\phi^\sigma}{2} - \sigma \gamma \operatorname{sgn} \left( \sin \frac{\phi^\sigma}{2} \right) \right) \right] \quad (11)$$

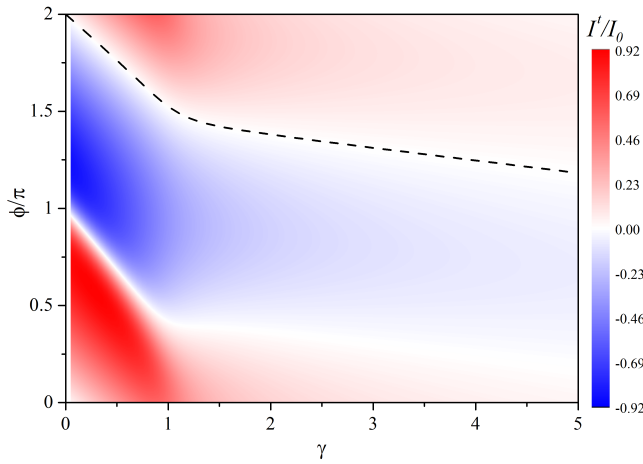


FIG. 3. Josephson current  $I^t$ , composed of the ABS and continuum states, carried by the top edge of the QSHI-based junction plotted as a function of the phase difference  $\phi$  and parameter  $\gamma = v_{FPS}/(2\Delta) \propto B$ . The dashed line traces the evolution of the superconducting phase difference  $\phi$  that minimizes the top-edge free energy at a given value of  $\gamma$ . Here  $k_B T = 0.1\Delta$ ,  $L_N \Delta/\hbar v_F = 0.1$  and the current  $I^t$  is measured in units of  $I_0 = e\Delta/(2\hbar)$ .

and

$$I_{\text{cont}}^{\sigma}(\phi^{\sigma}, T) = -I_0 \frac{\sigma}{\Delta} \frac{1}{\pi} \int_1^{\infty} dx \ln \left[ \frac{\cosh(\tilde{\Delta}(x + \gamma))}{\cosh(\tilde{\Delta}(x - \gamma))} \right] \\ \times \frac{x^2 \cos \phi^{\sigma} - \cos^2 \frac{\phi^{\sigma}}{2}}{\sqrt{x^2 - 1} (x^2 - \cos^2 \frac{\phi^{\sigma}}{2})^2}. \quad (12)$$

At zero magnetic field,  $\gamma$  reduces to zero and consequently Eq. (12) gives no contribution, which is consistent with the expectation that in field-free short junctions the supercurrent is driven by the sub-gap states.

Figure 3 shows the top-edge current-phase relation,  $I^t(\phi)$ , normalized to  $I_0$  at  $k_B T = 0.1\Delta$  as a function of the phase difference  $\phi$  and the dimensionless parameter  $\gamma \propto B$  [see Eq. (10)]. As  $\gamma$  increases, the maxima (red loci), minima (blue loci) and zeros (white trench) of the current-phase relation move along the  $\phi$  axis, while, simultaneously, the amplitude of the Josephson current

reduces.

It follows from Eq. (8), that the points  $(\gamma, \phi^t)$  where  $I^t$  vanishes and the free energy  $F^t$  minimizes—shown in Fig. 3 by the black-dashed line—determine the ground-state phase, i.e., the phase at which the top edge is in its ground state for a given  $\gamma$  (magnetic field). As shown in Fig. 3, increasing  $\gamma$  causes the ground-state phase to shift from  $2\pi$  ( $\sim 0$ ) to  $\pi$ , resulting in the top junction edge undergoing a  $0 - \pi$ -like transition. The second white trench seen in Fig. 3, emanating from  $\phi = \pi$  at  $\gamma = 0$ , corresponds to maxima of the free energy  $F^t$ . The supercurrent at the bottom edge can readily be obtained from Fig. 3 by using the symmetry relation  $I^b(\phi, \gamma) = -I^t(2\pi - \phi, \gamma)$ .

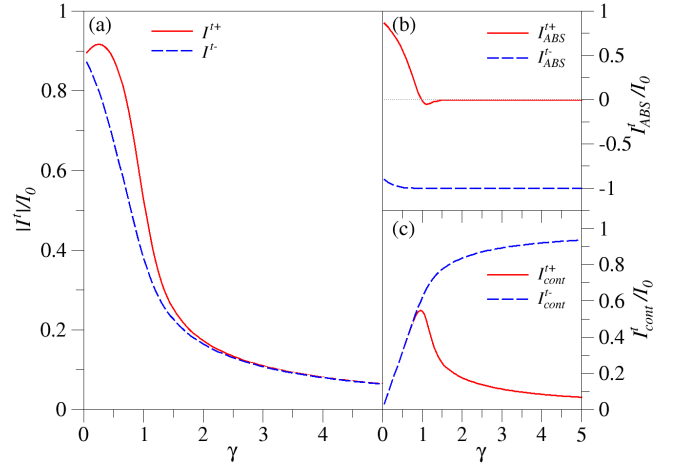


FIG. 4. Top edge Josephson current characteristics for QSHI-based JJ. Panel (a) displays maximal (red),  $I^{t+}$ , and minimal (blue),  $I^{t-}$ , critical currents (normalized to  $I_0$ ) as functions of  $\gamma = v_{FPS}/(2\Delta) \propto B$ . Panels (b) and (c) show, correspondingly, the ABS contribution,  $I_{\text{ABS}}^{t\pm}$ , and continuum-state contribution,  $I_{\text{cont}}^{t\pm}$ , of  $I^{t\pm}$ . Again the maxima and minima are plotted in red and blue.

In the low-temperature limit, the integration in Eq. (12) can be performed analytically and the contribution from the continuum of states at the top/bottom edge reduces to

$$I_{\text{cont}}^{\sigma}(\phi^{\sigma}, T \rightarrow 0) = \sigma \frac{2I_0}{\pi} \left\{ \gamma + \Theta(\gamma - 1) \left[ \arctan \left( \frac{\sqrt{\gamma^2 - 1}}{\sin \frac{\phi^{\sigma}}{2}} \right) \sin \frac{\phi^{\sigma}}{2} - \sqrt{\gamma^2 - 1} \right] \right\}. \quad (13)$$

Note that the above equation has been derived assuming  $B \geq 0$  or equivalently  $\gamma \geq 0$ . To obtain the corresponding expression for  $B < 0$ , the relation  $I^{\sigma}(B, \phi) = I^{-\sigma}(-B, \phi)$  can be used. It is instructive to connect the dependence of  $I_{\text{cont}}^{\sigma}(\phi^{\sigma}, T \rightarrow 0)$  on  $\gamma$  with the closing of

the effective superconducting gap, see Fig. 2(b), and of the lifting of the protected ABS crossing, see Fig. 2(c), when  $\gamma = v_{FPS}/(2\Delta)$  exceeds unity.

#### IV. SUPERCONDUCTING DIODE EFFECT AND $Q$ -FACTOR

The maximum  $I^{\sigma+} = \max_{\phi^\sigma} I^\sigma(\phi^\sigma)$  and minimum  $I^{\sigma-} = \min_{\phi^\sigma} I^\sigma(\phi^\sigma)$  of the total Josephson current for a given edge,  $\sigma$ , at a given magnetic field  $B \propto \gamma$  determine the  $Q$ -factor,  $Q^\sigma(\gamma, T)$ . The latter serves as a

$$Q^\sigma(\gamma, T \rightarrow 0) = \sigma \left\{ \left( \sqrt{1 - \gamma^2} - 1 + \frac{4\gamma}{\pi} \right) \Theta(1 - \gamma) + \left[ \frac{4}{\pi} \left( \gamma - \sqrt{\gamma^2 - 1} \right) + \frac{2}{\pi} \arctan \left( \sqrt{\gamma^2 - 1} \right) - 1 \right] \Theta(\gamma - 1) \right\}. \quad (15)$$

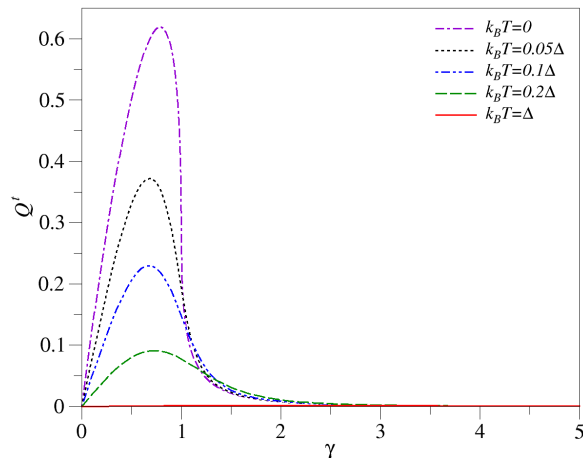


FIG. 5. Diode effect  $Q$ -factor, Eq. (14), for the top edge of QSHI-based JJ as a function of  $\gamma \propto B$  displayed for different temperatures. Here  $Q^t(T \rightarrow 0)$  is computed by means of Eq. (15).

Figure 4 illustrates the behavior of the Josephson current on the top edge. In particular, the maximal and minimal Josephson currents,  $I^{t+}$  and  $I^{t-}$ , are displayed in Fig. 4(a) as functions of  $\gamma \propto B$ , while different contributions to  $I^{t\pm}$ , carried by the ABS and continuum states, are plotted in Figs. 4(b) and (c). As already observed in Fig. 3, the Josephson current gets suppressed with increasing  $\gamma$ , and thus also  $I^{\sigma\pm}$ . Consequently, the  $Q$ -factor is expected to approach zero when  $\gamma$  increases.

This is borne out by Fig. 5, which shows the  $Q$ -factor

figure of merit quantifying the SDE as a function of the out-of-plane field and temperature,

$$Q^\sigma(\gamma, T) = \frac{|I^{\sigma+}| - |I^{\sigma-}|}{I_0}. \quad (14)$$

Combining the low-temperature limit of Eq. (11) with Eq. (13), yields,

of the top edge for different temperatures. According to Eq. (15), the  $Q$ -factor at  $T = 0$  exhibits a pronounced maximum  $Q_{\max}^t = \sqrt{16/\pi^2 + 1} - 1 \approx 0.618993$  at  $\gamma_{\max} = 1/\sqrt{1 + \pi^2/16} \approx 0.786439$ . The fact that both  $Q_{\max}^t$  and  $\gamma_{\max}$  reduce to universal values, independent of junction parameters, is quite remarkable.<sup>46</sup> As  $T$  increases, the  $Q$ -factor decreases until the pronounced peak observed at low temperatures is no longer discernible [see, for example, the solid line corresponding to  $k_B T = \Delta$  in Fig. 5].

It is clear from Eq. (15) that the net  $Q$ -factor of the narrow topological JJs, consisting of top and bottom edges,  $Q_{\text{tot}} = Q^t + Q^b$ , vanishes because  $Q^t = -Q^b$  (see also Appendix B). Hence, to realize a finite SDE in QSHI-based junctions, a setup with disparate QSHI edges is required. This can be achieved, for example, by using the setup depicted in Fig. 1(a), where the superconductor proximitizes only one edge (the top edge in this case), or by designing the heterojunction in a way that the corresponding Fermi velocities  $v_F^t$  and  $v_F^b$  become substantially different.

#### V. PARITY CONSERVING SUPERCONDUCTING DIODE EFFECT

Having discussed the SDE in a situation without constraints on the fermion parity, we now discuss a scenario in which the fermionic ground-state parity is conserved. To keep track of that, all underlying quantities are indexed by the subscript  $p$ . Correspondingly, the parity-conserved free energy—up to phase-independent contributions—reads,<sup>43,47,48</sup>

$$F_p^\sigma(\phi^\sigma, T) = F^\sigma(\phi^\sigma, T) - k_B T \ln \left\{ \frac{1}{2} \left[ 1 + p P_\sigma(\phi^\sigma) \tanh \left| \frac{\epsilon_+^\sigma(\phi^\sigma)}{2k_B T} \right| \exp \left[ J_S(T) + \int_0^\infty d\epsilon \rho_{\text{tot}}^\sigma(\epsilon, \phi^\sigma) \ln \left[ \tanh \left( \frac{\epsilon}{2k_B T} \right) \right] \right] \right] \right\}, \quad (16)$$

where the equilibrium free energy  $F^\sigma(\phi^\sigma, T)$  is given by Eq. (6) and the parity factor equals,

$$P_\sigma(\phi^\sigma) = \text{sgn} \left[ \cos \frac{\phi^\sigma}{2} - \sigma \gamma \text{sgn} \left( \sin \frac{\phi^\sigma}{2} \right) \right]. \quad (17)$$

The above form of  $P_\sigma(\phi^\sigma)$  implies a convention according to which the fermionic parity  $p = +1$  corresponds to the lower, and  $p = -1$  to the upper spectral branches

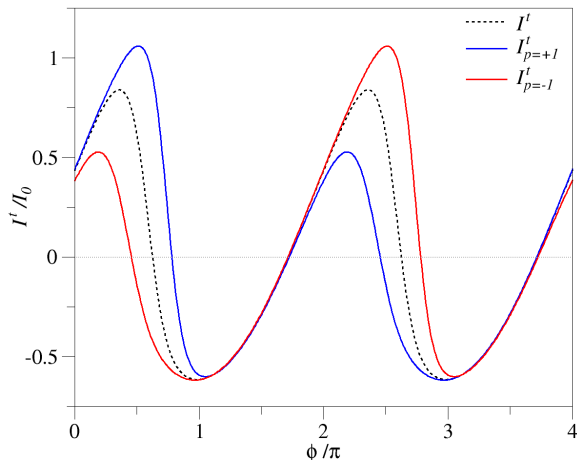


FIG. 6. Josephson current carried by the top edge of QSHI-based JJ plotted as a function of the phase difference  $\phi$  with (solid lines) and without (dashed line) parity constraints:  $I^t$  stands for parity unconstrained  $2\pi$  periodic current, Secs. II-IV, while  $I_{p=\pm 1}^t$  denotes parity conserved  $4\pi$  periodic currents with  $p = \pm 1$ . Here  $\gamma = 0.6$ ,  $k_B T = 0.1\Delta$ ,  $E_S = 0.05\Delta$ ,  $L_N \Delta / \hbar v_F = 0.1$  and the currents are measured in units of  $I_0 = e\Delta / (2\hbar)$ .

in Fig. 2, where lower and upper refer to energies near  $\phi = 0$ .

In contrast to the Josephson current  $I^\sigma(\phi^\sigma, T)$  derived from the equilibrium free energy  $F^\sigma(\phi^\sigma, T)$ , the parity conserving Josephson current  $I_p^\sigma(\phi^\sigma, T)$  derived from  $F_p^\sigma(\phi^\sigma, T)$  via Eq. (8), involves the total quasi-particle DOS,  $\rho_{\text{tot}}^\sigma(\epsilon, \phi^\sigma) = \rho^\sigma(\epsilon, \phi^\sigma) + \bar{\rho}_0(\epsilon)$ , which in addition to the term  $\rho^\sigma(\epsilon, \phi^\sigma)$  given by Eq. (7) contains the phase-independent contribution,

$$\bar{\rho}_0(\epsilon) = \frac{2}{\pi E_S} \sum_{s=\uparrow/\downarrow} \frac{|\epsilon_s| \Theta(\epsilon_s^2 - \Delta^2)}{\sqrt{\epsilon_s^2 - \Delta^2}}, \quad (18)$$

where the energy scale,  $E_S = \hbar v_F / L_S$ , is related to the total length  $L_S$  of the superconducting QSHI edge. In a similar way, the  $\phi$ -independent DOS of the superconducting electrodes on top of the QSHI contribute with<sup>49</sup>

$$J_S(T) = -\frac{2}{\pi k_B T E_S} \int_{\Delta}^{\infty} d\epsilon \frac{\sqrt{\epsilon^2 - \Delta^2}}{\sinh(\epsilon/k_B T)}. \quad (19)$$

Although the underlying expressions get more involved when compared to Secs. III-IV, still some approximate analytical results can be obtained in the limiting case  $T \rightarrow 0$  and  $\gamma \ll 1$ . However, one needs to pay an attention in which order are the corresponding mathematical operations taken into action: first goes an integration in Eq. (16), then derivative with respect to  $\phi$  and finally the limit  $T \rightarrow 0$ . Proceeding in this way, the current for a fixed fermionic parity  $p = \pm 1$  reduces to

$$I_p^\sigma(\phi^\sigma, T \rightarrow 0) = \sigma I_0 \left( p \sin \frac{\phi^\sigma}{2} + \frac{2\gamma}{\pi} \right), \quad \gamma \ll 1 \quad (20)$$

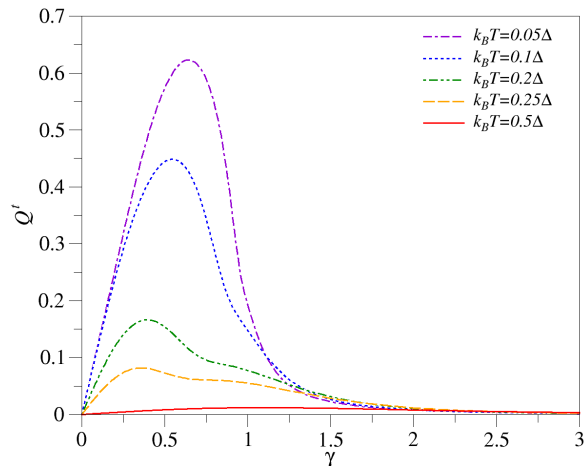


FIG. 7. Diode effect  $Q$ -factor, Eq. (14), for the top edge of QSHI-based JJ with the parity  $p = +1$  as a function of  $\gamma \propto B$  and different temperatures. Here  $E_S = 0.05\Delta$ . Note that the  $Q$ -factor for  $p = -1$  is the same as that for  $p = +1$ .

with the corresponding  $Q$ -factor [see Eq. (14)]

$$Q_p^\sigma(\gamma, T \rightarrow 0) = \sigma \frac{4\gamma}{\pi}, \quad \gamma \ll 1. \quad (21)$$

While Eqs. (20) and (21) already provide some useful guidance, we proceed fully numerically for a more detailed analysis.

Figure 6 shows the parity conserving Josephson currents,  $I_{p=\pm 1}^t(\phi^\sigma, T)$ , at the top edge, for both fermionic parities  $p = \pm 1$ . In contrast to the parity unconstrained Josephson current,  $I^t(\phi^\sigma, T)$ , which exhibits  $2\pi$  periodicity, its parity-conserved counterpart,  $c$ , becomes  $4\pi$  periodic.<sup>43,47,48</sup> Moreover, Fig. 6 illustrates how for  $\gamma < 1$  the asymmetry between the magnitudes of the maximal and minimal values of the Josephson current increases when the fermionic ground-state parity is kept conserved. This, in turn, implies that for  $\gamma < 1$  parity conservation enhances the SDE, as evidenced by Fig. 7, where the magnetic-field dependence of the  $Q$ -factor [see Eq. (14)] is shown for  $p = +1$  and various temperatures. Indeed, by comparing Figs. 5 and 7 we can observe that, at a given temperature, the parity-conserved  $Q$ -factor is generally larger than its parity-unconstrained counterpart, as long as the magnetic field keeps the global superconducting gap open (that is, when  $\gamma < 1$ ). However, when  $\gamma \geq 1$ , the additional contributions in Eq. (16) tend to zero and  $F_p^\sigma(\phi^\sigma, T)$  tends to the equilibrium free energy  $F^\sigma(\phi^\sigma, T)$ . Therefore, the  $Q$ -factors for the case with and without fermionic parity conservation approach each other when  $\gamma \geq 1$ . For low temperatures,  $Q$  increases linearly (see Fig. 7), which is perfectly described by Eq. (21).

While we predict that for magnetic fields such that  $\gamma < 1$ , topological JJs with conserved fermionic parity exhibit larger  $Q$ -factors than their parity unconstrained counter-

parts, their experimental realization becomes more challenging, as will be discussed in the following section.

## VI. EXPERIMENTAL REALIZATIONS

Turning to potential experimental realizations displaying the SDE, we first consider the situation, where the fermionic ground-state parity does not play a role. As discussed above, if both edges of the QSHI-based JJ are equivalent [e.g., as illustrated in Fig. 1(b)], their contributions to the SDE cancel each other out. One way to overcome this difficulty is to design the system so that the two edges of the JJ become nonequivalent. For example, by predominantly transporting Cooper pairs along one edge, as shown in Fig. 1(a). In this configuration, only the top edge constitutes a short JJ, while the bottom edge forms a long JJ that carries less current due to a diminished contribution from the ABS. Consequently, the  $Q$ -factor is dominated by that of the top edge, making the single-edge physics discussed in Sec. IV experimentally relevant.

Another way to make the edges nonequivalent is by endowing them with different Fermi velocities. For instance, in  $\text{Hg}_{1-x}\text{Cd}_x\text{Te}/\text{HgTe}/\text{Hg}_{1-x}\text{Cd}_x\text{Te}$ -based quantum wells realizing a QSHI, the bandgap and Fermi velocity depend on (i) the thickness of the HgTe spacer, and (ii) the stoichiometric ratio of the Cd compound. Therefore, manufacturing HgTe-based quantum wells with different thicknesses and/or different Cd concentrations at opposite edges will make the edges nonequivalent, resulting in an observable non-zero SDE.

While we anticipate a finite SDE for QSHI-junctions with a single edge or non-equivalent edges in a situation without parity constraints, preserving the fermionic parity of the ground state in experimental setups poses additional challenges, requiring conducting experiments on timescales shorter than the quasi-particle poisoning rate.<sup>50,51</sup> For the topological JJs based on  $\text{Hg}_{1-x}\text{Cd}_x\text{Te}/\text{HgTe}/\text{Hg}_{1-x}\text{Cd}_x\text{Te}$  such timescales become of the order of  $1\ \mu\text{s}$ .<sup>52-54</sup> Consequently, experiments aiming to measure the parity-conserving SDE must operate within a sub- $\mu\text{s}$  range. Nevertheless, with modern qubit and SQUID technologies enabling controlled modulation of  $\phi$  on timescales of 1 ns or shorter<sup>55</sup>, the observation of a parity-conserving SDE in narrow topological JJs, despite being challenging, should be experimentally feasible.

## VII. CONCLUSIONS

In this work we have studied the SDE in narrow topological QSHI-based JJs triggered by an out-of-

plane magnetic field. In general, the realization of the SDE in QSHI-based JJs requires the transport of Cooper pairs through nonequivalent edge channels at the opposite ends of the junction. We investigated two different parity regimes—the conventional, so-called parity-unconstrained regime and a novel one, where the fermionic parity of the ground state is preserved. Our findings demonstrate that QSHI-based JJs can be used as versatile experimental platforms showcasing the SDE. Furthermore, our calculations predict an increase in the  $Q$ -factor and, consequently, the diode efficiency as the temperature decreases. Interestingly, in the parity-unconstrained low-temperature regime, the maximum diode efficiency exhibits a universal character, with the maximum  $Q$ -factor value being independent of the system and Hamiltonian parameters. This remarkable behavior appears to be a direct consequence of the topological nature of edge-state charge transport in the QSHI regime.

Complementary to detailed numerical simulations, we also provide valuable analytical results that can be readily applied to understanding, interpreting, and fitting experimental data.

## ACKNOWLEDGMENTS

D.K. acknowledges partial support from the project IM-2021-26 (SUPERSPIN) funded by the Slovak Academy of Sciences via the programme IMPULZ 2021, and VEGA Grant No. 2/0156/22—QuaSiModo. A.M.A. acknowledges support from ONR Grant No. N000141712793.

### Appendix A: Alternative definition of $Q$ -factor

In addition to the definition of the  $Q$ -factor as given in Eq. (14), one can alternatively define the  $Q$ -factor as

$$Q_{\text{alt}}^{\sigma}(\gamma, T) = \frac{|I^{\sigma+}| - |I^{\sigma-}|}{|I^{\sigma+}| + |I^{\sigma-}|}, \quad (\text{A1})$$

where  $I^{\sigma+}$  and  $I^{\sigma-}$  are the global maxima and minima of the Josephson current, respectively. The dependence of  $Q_{\text{alt}}^t(\gamma, T)$  on  $\gamma$  is shown in Fig. 8 for different values of the temperature. In the zero-temperature limit the  $Q$ -factor defined by Eq. (A1) can be written as,

$$Q_{\text{alt}}^{\sigma}(\gamma, T \rightarrow 0) = \sigma \left\{ \frac{\sqrt{1-\gamma^2} - 1 + 4\gamma/\pi}{\sqrt{1-\gamma^2} + 1} \Theta(1-\gamma) + \left[ \frac{2(\gamma - \sqrt{\gamma^2 - 1})}{\pi/2 - \arctan(\sqrt{\gamma^2 - 1})} - 1 \right] \Theta(\gamma - 1) \right\}. \quad (\text{A2})$$

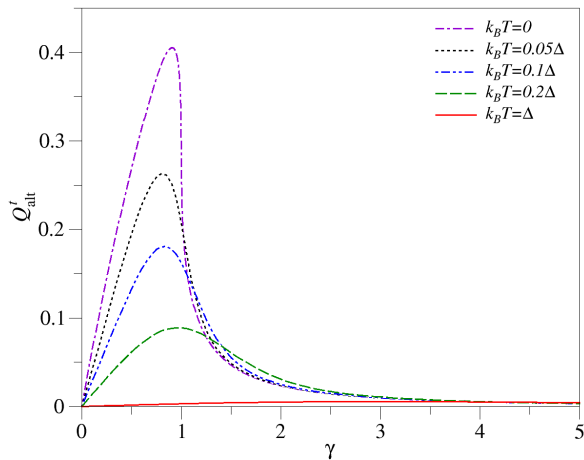


FIG. 8.  $Q$ -factor of the top edge,  $Q_{\text{alt}}^t$ , see Eq. (A1), as a function of  $\gamma = v_{FPS}/(2\Delta) \propto B$  for different temperatures.  $Q(T \rightarrow 0)$  is computed from Eq. (A2).

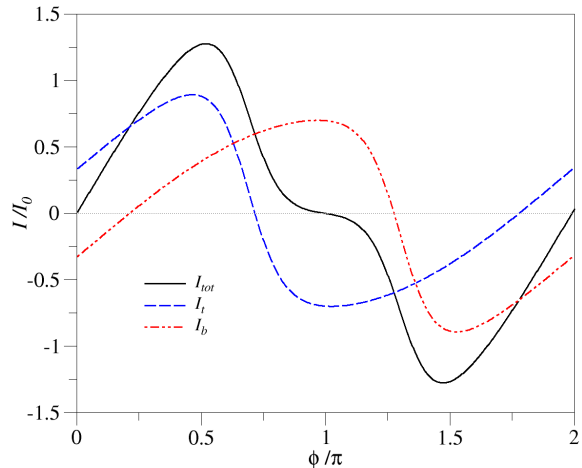


FIG. 9. Total Josephson current (black) of a QSHI-based JJ and the individual contributions from the top (blue) and bottom (red) edges as a function of the phase difference  $\phi$ . Here  $v_{FPS} = 0.9\Delta$  and  $L_N\Delta/\hbar v_F = 0.1$ .

### Appendix B: Josephson current at the top and bottom edges

As discussed in the main text, if the edge states at the opposite ends (say, top and bottom) of the QSHI-based JJ are equivalent, the SDE contribution at the top and bottom edges cancel each other out, leading to a vanishing  $Q$ -factor. This is illustrated in Fig. 9, where the total Josephson current,  $I_{\text{tot}}(\phi, T) = I^t(\phi, T) + I^b(\phi, T)$ , as well as the individual contributions from the top and bottom edges are shown. When the edges are equivalent, their associated currents  $I^t(\phi, T)$  and  $I^b(\phi, T)$  obey the symmetry relation,  $\max[I_{\text{tot}}(\phi, T)] = |\min[I_{\text{tot}}(\phi, T)]|$ , which in turn implies that  $Q_{\text{tot}} = 0$ .

\* corresponding author: denis.kochan@savba.sk

<sup>1</sup> M. Nadeem, M. S. Fuhrer, and X. Wang, *Nature Reviews Physics* **5**, 558 (2023).

<sup>2</sup> A. G. Sivakov, O. G. Turutanov, A. E. Kolinko, and A. S. Pokhila, *Low Temperature Physics* **44**, 226 (2018).

<sup>3</sup> D. Y. Vodolazov, A. Y. Aladyshkin, E. E. Pestov, S. N. Vdovichev, S. S. Ustavshikov, M. Y. Levichev, A. V. Putilov, P. A. Yunin, A. I. El'kina, N. N. Bukharov, and A. M. Klushin, *Supercond. Sci. Technol.* **31**, 115004 (2018).

<sup>4</sup> F. Ando, Y. Miyasaka, T. Li, J. Ishizuka, T. Arakawa, Y. Shiota, T. Moriyama, Y. Yanase, and T. Ono, *Nature* **584**, 373 (2020).

<sup>5</sup> Y. Hou, F. Nichele, H. Chi, A. Lodesani, Y. Wu, M. F. Ritter, D. Z. Haxell, M. Davydova, S. Ilić, O. Glezakou-Elbert, A. Varambally, F. S. Bergeret, A. Kamra, L. Fu, P. A. Lee, and J. S. Moodera, *Phys. Rev. Lett.* **131**, 027001 (2023).

<sup>6</sup> C. Baumgartner, L. Fuchs, A. Costa, S. Reinhardt, S. Gronin, G. C. Gardner, T. Lindemann, M. J. Manfra, P. E. Faria Junior, D. Kochan, J. Fabian, N. Paradiso, and C. Strunk, *Nature Nanotechnology* **17**, 39 (2022).

<sup>7</sup> C. Baumgartner, L. Fuchs, A. Costa, J. Picó-Cortés, S. Reinhardt, S. Gronin, G. C. Gardner, T. Lindemann, M. J. Manfra, P. E. F. Junior, D. Kochan, J. Fabian,



- N. Paradiso, and C. Strunk, *Journal of Physics: Condensed Matter* **34**, 154005 (2022).
- <sup>8</sup> B. Turini, S. Salimian, M. Carrega, A. Iorio, E. Strambini, F. Giazotto, V. Zannier, L. Sorba, and S. Heun, *Nano Letters* **22**, 8502 (2022).
- <sup>9</sup> A. Costa, C. Baumgartner, S. Reinhardt, J. Berger, S. Gronin, G. C. Gardner, T. Lindemann, M. J. Manfra, J. Fabian, D. Kochan, N. Paradiso, and C. Strunk, *Nature Nanotechnology* **18**, 1266 (2023).
- <sup>10</sup> N. Lotfizadeh, W. F. Schiela, B. Pekerten, P. Yu, B. H. Elfeky, W. M. Strickland, A. Matos-Abiague, and J. Shabani, *Commun. Phys.* **7**, 120 (2024).
- <sup>11</sup> S. Reinhardt, T. Ascherl, A. Costa, J. Berger, S. Gronin, G. C. Gardner, T. Lindemann, M. J. Manfra, J. Fabian, D. Kochan, C. Strunk, and N. Paradiso, *Nature Communications* **15**, 4413 (2024).
- <sup>12</sup> B. Pal, A. Chakraborty, P. K. Sivakumar, M. Davydova, A. K. Gopi, A. K. Pandeya, J. A. Krieger, Y. Zhang, M. Date, S. Ju, N. Yuan, N. B. M. Schröter, L. Fu, and S. S. P. Parkin, *Nature Physics* (2022).
- <sup>13</sup> K.-R. Jeon, J.-K. Kim, J. Yoon, J.-C. Jeon, H. Han, A. Cottet, T. Kontos, and S. S. P. Parkin, *Nature Materials* **21**, 1008 (2022).
- <sup>14</sup> R. Wakatsuki, Y. Saito, S. Hoshino, Y. M. Itahashi, T. Ideue, M. Ezawa, Y. Iwasa, and N. Nagaosa, *Science Advances* **3**, e1602390 (2017).
- <sup>15</sup> H. Wu, Y. Wang, Y. Xu, P. K. Sivakumar, C. Pasco, U. Filippo, S. S. P. Parkin, Y.-J. Zeng, T. McQueen, and M. N. Ali, *Nature* **604**, 653 (2022).
- <sup>16</sup> L. Bauriedl, C. Bäuml, L. Fuchs, C. Baumgartner, N. Paulik, J. M. Bauer, K.-Q. Lin, J. M. Lupton, T. Taniguchi, K. Watanabe, C. Strunk, and N. Paradiso, *Nature Communications* **13**, 4266 (2022).
- <sup>17</sup> J. D'íez-Mérida, A. D'íez-Carlón, S. Y. Yang, Y. M. Xie, X. J. Gao, J. Senior, K. Watanabe, T. Taniguchi, X. Lu, A. P. Higginbotham, K. T. Law, and D. K. Efetov, *Nature Communications* **14**, 2396 (2023).
- <sup>18</sup> J.-X. Lin, P. Siriviboon, H. D. Scammell, S. Liu, D. Rhodes, K. Watanabe, T. Taniguchi, J. Hone, M. S. Scheurer, and J. I. A. Li, *Nature Physics* **18**, 1221 (2022).
- <sup>19</sup> M. Trahms, L. Melischek, J. F. Steiner, B. Mahendru, I. Tamir, N. Bogdanoff, O. Peters, G. Reecht, C. B. Winkelmann, F. von Oppen, and K. J. Franke, *Nature* **615**, 628 (2023).
- <sup>20</sup> S. Banerjee and M. S. Scheurer, “Altermagnetic superconducting diode effect,” (2024), arXiv:2402.14071 [cond-mat.supr-con].
- <sup>21</sup> S.-B. Zhang, L.-H. Hu, and T. Neupert, *Nature Communications* **15**, 1801 (2024).
- <sup>22</sup> M. Davydova, S. Prembabu, and L. Fu, *Science Advances* **8**, eabo0309 (2022).
- <sup>23</sup> M. Coraiola, A. E. Svetogorov, D. Z. Haxell, D. Sabonis, M. Hinderling, S. C. ten Kate, E. Cheah, F. Krizek, R. Schott, W. Wegscheider, J. C. Cuevas, W. Belzig, and F. Nichele, *ACS Nano* **18**, 9221 (2024).
- <sup>24</sup> V. M. Edelstein, *Sov. Phys. - JETP* **68**, 1244 (1989).
- <sup>25</sup> V. M. Edelstein, *Journal of Physics: Condensed Matter* **8**, 339 (1996).
- <sup>26</sup> A. Daido, Y. Ikeda, and Y. Yanase, *Phys. Rev. Lett.* **128**, 037001 (2022).
- <sup>27</sup> N. F. Q. Yuan and L. Fu, *Proc. Natl. Acad. Sci. USA* **119**, e2119548119 (2022).
- <sup>28</sup> M. Smith, A. V. Andreev, and B. Z. Spivak, *Phys. Rev. B* **104**, L220504 (2021).
- <sup>29</sup> J. J. He, Y. Tanaka, and N. Nagaosa, *New J. Phys.* **24**, 053014 (2022).
- <sup>30</sup> H. D. Scammell, J. I. A. Li, and M. S. Scheurer, *2D Mater.* **9**, 025027 (2022).
- <sup>31</sup> S. Ilić and F. S. Bergeret, *Phys. Rev. Lett.* **128**, 177001 (2022).
- <sup>32</sup> T. de Picoli, Z. Blood, Y. Lyanda-Geller, and J. I. Väyrynen, *Phys. Rev. B* **107**, 224518 (2023).
- <sup>33</sup> L. Fuchs, D. Kochan, J. Schmidt, N. Hüttner, C. Baumgartner, S. Reinhardt, S. Gronin, G. C. Gardner, T. Lindemann, M. J. Manfra, C. Strunk, and N. Paradiso, *Phys. Rev. X* **12**, 041020 (2022).
- <sup>34</sup> A. Banerjee, M. Geier, M. A. Rahman, C. Thomas, T. Wang, M. J. Manfra, K. Flensberg, and C. M. Marcus, *Phys. Rev. Lett.* **131**, 196301 (2023).
- <sup>35</sup> A. Sundaresh, J. I. Väyrynen, Y. Lyanda-Geller, and L. P. Rokhinson, *Nature Communications* **14**, 1628 (2023).
- <sup>36</sup> D. Kochan, A. Costa, I. Zhumagulov, and I. Žutić, “Phenomenological Theory of the Supercurrent Diode Effect: The Lifshitz Invariant,” (2023), arXiv:2303.11975 [cond-mat.supr-con].
- <sup>37</sup> A. Costa, J. Fabian, and D. Kochan, *Phys. Rev. B* **108**, 054522 (2023).
- <sup>38</sup> V. Mineev and K. Samokhin, *JETP* **78**, 401 (1994).
- <sup>39</sup> O. Dimitrova and M. V. Feigel'man, *Phys. Rev. B* **76**, 014522 (2007).
- <sup>40</sup> A. Buzdin, *Phys. Rev. Lett.* **101**, 107005 (2008).
- <sup>41</sup> V. P. Mineev and M. Sigrist, in *Non-Centrosymmetric Superconductors*, edited by E. Bauer and M. Sigrist (Springer Berlin Heidelberg, 2012) pp. 129–154.
- <sup>42</sup> A. Costa, J. Fabian, and D. Kochan, *Physical Review B* **98**, 134511 (2018).
- <sup>43</sup> B. Scharf, A. Braggio, E. Strambini, F. Giazotto, and E. M. Hankiewicz, *Phys. Rev. Res.* **3**, 033062 (2021).
- <sup>44</sup> G. Tkachov, P. Buset, B. Trauzettel, and E. M. Hankiewicz, *Phys. Rev. B* **92**, 045408 (2015).
- <sup>45</sup> G. Tkachov, *Phys. Rev. B* **100**, 035403 (2019).
- <sup>46</sup> For the bottom edge, there is a minimum at  $\gamma = 1/\sqrt{1 + \pi^2/16}$  with a value of  $Q^b = -\sqrt{16/\pi^2 + 1} + 1$ .
- <sup>47</sup> P. A. Iosevich and M. V. Feigel'man, *Phys. Rev. Lett.* **106**, 077003 (2011).
- <sup>48</sup> C. W. J. Beenakker, D. I. Pikulin, T. Hyart, H. Schomerus, and J. P. Dahlhaus, *Phys. Rev. Lett.* **110**, 017003 (2013).
- <sup>49</sup> Assuming a quasi-particle density of states  $\rho_S(\epsilon) = 2/(\pi E_S)|\epsilon|\Theta(\epsilon^2 - \Delta^2)/\sqrt{\epsilon^2 - \Delta^2}$  from the superconducting electrodes, one can compute its contribution to Eq. (16) via  $J_S(T) = \int_0^\infty d\epsilon \rho_S(\epsilon) \ln \left[ \tanh \left( \frac{\epsilon}{2k_B T} \right) \right]$ , which yields Eq. (19), as detailed in Refs. 43 and 48.
- <sup>50</sup> R. M. Lutchyn, J. D. Sau, and S. Das Sarma, *Phys. Rev. Lett.* **105**, 077001 (2010).
- <sup>51</sup> C.-K. Chiu and S. Das Sarma, *Phys. Rev. B* **99**, 035312 (2019).
- <sup>52</sup> D. Rainis and D. Loss, *Phys. Rev. B* **85**, 174533 (2012).
- <sup>53</sup> P. Virtanen and P. Recher, *Phys. Rev. B* **88**, 144507 (2013).
- <sup>54</sup> D. Frombach and P. Recher, *Phys. Rev. B* **101**, 115304 (2020).
- <sup>55</sup> M. Mück and R. McDermott, *Supercond. Sci. Technol.* **23**, 093001 (2010).